BMC Musculoskeletal Disorders

RESEARCH

Open Access

Mitochondria derived from Stem cells modulated the biological behavior of monocyte-macrophages and inhibited inflammatory bone resorption

Xingfu Li[1,2], Jingyue Su[3,4], Xiang Liu[5], Wei Lu[1,2*] and Zhenhan Deng[3,4*]

Abstract

Background The transfer of mitochondria from stem cells effectively attenuates the viability of inflammatory cells. However, there is a paucity of research supporting the inhibitory effect of stem cells on inflammatory bone resorption through mitochondrial transfer.

Methods Mouse bone resorption models were established to investigate the impact of stem cell-derived mitochondria. Stem cells, stem cell-derived mitochondria and exosomes were injected into the animal models for experimental research. Healthy mice and mice with bone resorption were included as the control groups. The mitochondrial transfer and bone resorption of mice calvaria were evaluated by immunofluorescence, gross morphology, micro-computed tomography (micro-CT), immunohistochemical staining. Monocyte-macrophages were incubated with stem cell-derived mitochondria as experimental group. Monocyte-macrophages and activated monocyte-macrophages cultured separately served as the control groups. The mitochondrial transfer and biological behavior of monocyte-macrophages were evaluated by immunofluorescence, enzyme-linked immunosorbent assay (ELISA), Multiskan FC, and histochemical staining.

Results Stem cell-derived mitochondria were successfully transferred to monocyte-macrophages. In vivo, local injection of stem cells, mitochondria, and exosomes effectively mitigated inflammatory cell infiltration, suppressed osteoclast maturation, and demonstrated a higher relative bone volume in mouse bone resorption models compared to the negative control group. In vitro, the co-incubation of mitochondria effectively suppressed the secretion of inflammatory cytokines, proliferation, fusion, and osteoclastogenesis in monocyte-macrophages compared to the control groups.

Conclusions The modulation of monocyte-macrophages biological behaviors by stem cells may occur through the transfer of mitochondria, thereby mitigating inflammatory bone resorption.

Keywords Stem cell, Mitochondrial transfer, Inflammatory bone resorption

*Correspondence:
Wei Lu
weilu9309@gmail.com
Zhenhan Deng
dengzhenhan@wmu.edu.cn
Full list of author information is available at the end of the article

Introduction

Bone resorption is one of the main cause of musculoskeletal disorders, including fracture, osteoporosis and inflammatory arthritis, which would reduce the quality of life and increases the risk of disability [1–3]. For example, the successful outcome of internal fixation surgery relies heavily on the proper healing and shaping of the fracture site, while numerous studies have demonstrated that bone resorption exerts a profound impact on the process of fracture healing and shaping, thereby compromising the efficacy of internal fixation surgery [4, 5]. However, the pathological mechanism of bone resorption is still not fully understood. Some researchers have found that during the remodeling stage of bone, inflammatory cells infiltrated around the fracture site, such as monocytes, macrophages, lymphocytes, neutrophils, produce inflammatory factors, such as interleukin (IL)-1β, IL-6, IL-17, tumor necrosis factorF-α (TNF-α), receptor activator of nuclear factor kappa-B ligand (RANKL), macrophage colony-stimulating factor (M-CSF), which induce the differentiation and maturation of osteoclasts and lead to excessive absorption of bone graft. These would result in failure of the bone healing and shaping [6–8]. Therefore, inhibition of inflammatory cell viability may be an effective measure to avoid excessive inflammatory bone resorption.

Studies have found that mesenchymal stem cells (MSCs) can regulate the activity of inflammatory cells by releasing indoleamine 2, 3-dioxygenase (IDO), prostaglandin E2 (PGE2), exosomes (carrying miR-1260b), transforming growth factor β (TGF-β) and other components, reduce the synthesis and release of inflammatory factors, inhibit the differentiation and maturation of osteoclasts, and thus reduce bone resorption [9–11]. In addition, some researchers have found that MSCs could activate peroxisome proliferator-activated receptor-γ coactivator-1α (PGC-1α) in monocyte-macrophages through mitochondrial transfer to play an anti-inflammatory role. In particular, bone marrow-derived mesenchymal stem cells (BMSCs) could reduce oxidative stress and inflammatory cytokines of monocyte-macrophages through mitochondrial transfer [12–15]. However, there is a lack of relevant studies to verify whether stem cell could affect bone resorption through mitochondrial transfer.

Drugs that inhibit bone resorption have been widely used in clinical, such as bisphosphonate, raloxifene, salmon calcitonin, semi-synthetic derivatives of natural isoflavones, which are mainly used to treat chronic degenerative diseases such as osteoporosis and osteoarthritis, also inevitably increase the burden of liver and kidney [16–18]. However, there is no study to prove that the drugs mentioned above could be used to inhibit inflammatory bone resorption at the fracture site. Regarding bone resorption, it is generally believed that dysregulated inflammation leads to increased bone resorption and inhibition of bone formation [19, 20]. The interaction between inflammatory cells, such as monocyte-macrophages, and bone healing-related cells, such as MSCs, plays a pivotal role in the processes of bone formation and resorption [21, 22]. Although many studies have found that stem cells could be used to inhibit inflammatory responses, there are many ethical and legal restrictions on the application of stem cells, and there is a lack of research to support that the stem cells play a positive role in the process of inflammatory bone resorption at the fracture site [23, 24].

In the field of biomedical sciences, stem cells have been used to repair tissue damage, and mitochondrial transfer is an important mechanism for stem cells to play a role. However, there is a lack of evidence to demonstrate that stem cell therapy of bone resorption is related to mitochondrial transfer [25]. Previous investigations within this study have demonstrated that human synovial fluid-derived mesenchymal stem cells (hSF-MSCs) possess the capability to suppress TNF-α secretion by monocyte-macrophages, as well as attenuate the hyperactive phenotype and proliferation of T lymphocytes, thereby suggesting their potential in inhibiting inflammatory bone resorption. Furthermore, hSF-MSCs can be readily harvested without exacerbating tissue damage in volunteers and exhibit robust proliferation capabilities for the extraction of high-quality mitochondria [26, 27]. Based on the principle that inflammatory cells influence osteoclast differentiation and maturation, this study aimed to investigate the potential of hSF-MSCs-derived mitochondria in modulating inflammatory cells and elucidate the mechanism underlying the inhibition of inflammatory bone resorption by stem cell-derived mitochondrial transfer. These findings will provide a novel theoretical foundation for utilizing stem cells in clinical settings to prevent excessive bone resorption during the process of fracture healing and shaping.

Materials and methods

Bone resorption model

C57BL/6J mice were provided by the Animal Laboratory Center of Peking University Graduate School. The animal experiments in this study were carried out with the informed consent obtained from the Ethics Committee of Peking University Graduate School.

C57BL/6J Mice keep the prone decubitus after induction using isoflurane. The anesthesia mask was fixed by pointing at the nose and mouth of the mice. At the same time, the maintenance channel of the anesthesia machine was opened, and the concentration and flow of isoflurane

were adjusted to achieve the maintenance level of anesthesia. After anesthesia, the limbs of the C57BL/6J mice were fixed and sterilized to fully expose the surgical field of the skull of the mice. The skin was cut along the sagittal line in the middle of the calvaria, and the size of the incision was about 0.5 cm. The periosteum of the skull was exposed, and lipopolysaccharide (LPS) solution (10 mg/mL) derived from Escherichia coli serotype O55:B5 (Solarbio, China) was injected into the skull subperiosteum according to the dose of 25mg/kg. After hemostasis of the surgical field, the skin was sutured and sterilized. Then, the mice were consistently bred in specific pathogen-free (SPF) animal research facilities. Seven days after the initial procedure, the bone resorption model mice were successfully established [28]. The bone resorption model mice were randomly divided into 5 groups (n = 5/group): the normal control group (NC group), the negative control group (PBS group) treated with phosphate buffer saline (PBS) injection, the mesenchymal stem cells group (MSCs group) treated with MSCs injection, the mitochondria group (Mito group) treated with mitochondria (Mito) injection, and the exosome group (Exo group) treated with exosome (Exo) injection.

Isolation and culture of hSF-MSCs

The human synovial fluid (hSF) samples were provided by XXBLINDEDXX and processed within 6 hours after collection.

The hSF samples were filtered through a 70 μm strainer (Cell Strainer, BD Falcon) to eliminate visible debris. The hSF samples were collected in 50 mL centrifuge tubes and centrifuged at 1000 rpm for 10 minutes at 4 ℃. The cell pellets were collected and resuspended with fresh medium [DMEM-basic, 10% exosome-free FBS (Sigma, USA), 0.1 mg/mL P/S (Sigma-Aldrich, USA)]. The cells were inoculated into T25 culture flask with 5 ml of fresh medium at a density of 3.0×10^4 cells/cm^2. The cells were incubated in an incubator with 5 % CO_2. After 3 days, the cultrue medium was changed and cells were washed with PBS [29]. Then the cultrue medium was changed every three days until the cells reached 70% confluency. The cells were resuspended using 0.25% EDTA trypsin (Life Technologies, USA) and seeded in new culture flasks. The cells were passaged several times until reach the requirement of our experiment.

Identification of hSF-MSCs

The flow cytometry (FC) was used for the detection of surface markers on hSF-MSCs. The hSF-MSCs were resuspended with PBS and stained with CD105, CD73,CD90, CD34, CD45, HLA-DR, CD11b and CD19 (BD Bioscience). The IgG-PE and IgG-FITC were used as control. Samples were analyzed using a FACSCanto II flow cytometer (Beckman) [30]. After the detection of surface markers, hSF-MSCs were induced in differentiation medium including chondrogenic, adipogenic, and osteogenic differentiation medium, to characterize the multi-directional differentiation potential [31]. Trilineagespecific markers were respectively analyzedusing toluidine blue (TB), alizarin red and Oil Red O after induction.

Extraction and characterization of mitochondria derived from stem cells

The third generation (P3) of hSF-MSCs were washed twice with PBS, cells were digested with trypsin cell digest solution, centrifuged at 200 g for 5 minutes at room temperature, and cells were collected. The cell precipitate was gently resuspended in PBS precooled in an ice bath, a small number of cells were taken for counting, the remaining cells were centrifuged at 600 g for 5 minutes at 4°C to precipitate the cells, and the supernatant was discarded. 1-1.5 mL of mitochondrial separator supplemented with phenyl methane sulfonyl fluoride (PMSF) was added to 10 to 30 million cells, cells were gently suspended and placed in an ice bath for 10 to 15 minutes. Transfer the cell suspension to a suitably sized glass homogenizer and homogenize for about 10-20 cycles. The cell homogenates were centrifuged at 1000g for 10 minutes at 4°C [32]. The supernatant was carefully transferred to another centrifuge tube and centrifuged at 3500g at 4°C for 10 minutes. The supernatant was carefully removed, and the precipitate was the isolated stem cell mitochondria.

Freshly extracted mitochondria were resuspended in 2.5 % glutaraldehyde electron microscope fixative and stored at 4°C. After 30 minutes, the morphology of mitochondria was observed by transmission electron microscopy (TEM) and pictures were taken [33]. Freshly extracted mitochondria were used to identify mitochondrial marker protein (TOMM22) by western blot (WB) [34].

Extraction and characterization of exosome derived from stem cells

The culture supernatant of hSF-MSCs (P3) was collected and centrifuged at 2,000 g for 10 minutes to remove cellular debris. The resulting supernatant was purified by centrifugation at 10,000 g for 30 minutes to remove cellular microvesicles. Subsequently, the resulting supernatant was filtered through 0.22 mm pore filters and subjected to centrifugation at 100,000 g for 70 minutes using a Beckman Coulter OptimaXPN-100 centrifuge to collect exosome pellets. The exosome pellets were resuspended in 30 mL of PBS and subsequently subjected to centrifugation at 100,000 g for 70 minutes to purify exosomes

[35]. The purified exosome pellets were resuspended in 100 μL of PBS and stored at -80℃.

For morphological analysis, the exosomes were applied onto formvar carbon-coated nickel grids. Subsequently, it was negatively stained with 2% uranyl acetate for a duration of 10 minutes, air-dried, and visualized using TEM (JEM-2000EX TEM, JEOL Ltd., Tokyo, Japan). For size distribution analysis, exosomes were diluted to a concentration of 500 ng/mL, and their sizes were determined using fast video capture and particle-tracking software on the NanoSight NS300 platform (Malvern Instruments) according to Nanoparticle Tracking Analysis (NTA). For specific surface antigen analysis, the exosomes were resuspended in 300 μL of PBS and stained with anti-CD63-FITC antibodies (BD Bioscience) [36]. IgG-FITC was utilized as a control. Subsequently, the samples were analyzed using a FACSCanto II flow cytometer (Beckman).

Detection of mitochondrial transfer in vivo and in vitro

In vivo, 10μL monocyte-macrophage tracer liposome Dil Liposome (10 μM) was injected into the bone resorption site of mice. Mitotracker Green (200 nM) was used to label the mitochondria in hSF-MSCs, and fresh mitochondria were extracted as described above. Then, green fluorescently labeled mitochondria were injected into sites of bone resorption in mice. After 24 hours, the mice were euthanized with carbon dioxide, and the soft tissue at the bone resorption site was dissected and placed in a 1.5 mL EP tube. Then, 0.5 μL viable cell nucleating solution (Hoechst 33258, 0.5 mg/mL) was added and incubated in the dark for 15 minutes. The soft tissue was made into frozen sections with a thickness of 3 μM, and the frozen sections were observed by laser confocal microscope [37]. The excitation wavelength was set at 549 nm, and the emission wavelength was set at 565 nm to observe the distribution of monocytes macrophages. The excitation wavelength was set at 488 nm, and the emission wavelength was set at 507 nm to observe the distribution of mitochondria.

In vitro, hSF-MSCs were stained for 45 minutes at room temperature with 200 nM Mitotracker Green FM (Invitrogen, Carlsbad, CA, USA) and monocyte- macrophage were stained with 500 nM Mitotracker Deep Red FM (Invitrogen, Carlsbad, CA, USA). The cells were washed three times with PBS and then continued to culture for 24 hours. The mitochondria derived from hSF-MSCs were collected according to the above method and co-incubated with monocyte- macrophage. After 24 hours, monocyte-macrophage were fixed using 4% paraformaldehyde at room temperature for a duration of 15 minutes. They were then rinsed three times followed by a 10-minute staining process utilizing 1 μg/ml DAPI (Invitrogen, Carlsbad, CA, USA) [38]. Ultimately, the condition of mitochondrial transfer was inspected using a laser confocal microscope (Leica, Wetzlar, Germany) .

Injection of stem cell, mitochondria, and exosome

The mitochondria suspension (100 μL), isolated from hSF-MSCs (1×10^6), were administered via injection into the bone resorption sites of the bone resorption model mice at a concentration of 1×10^8/100 μL, following the specified protocol. The administration of hSF-MSCs suspension (1×10^6/100 μL), exosomes suspension (1×10^9/100 μL) extracted from the culture supernatant of hSF-MSCs (1×10^6), and PBS were performed via injection into bone resorption sites in three separate groups of mice at an equal volume [28]. The injections into the bone resorption model mice were administered every three days for a total duration of 12 days.

Gross view and micro-computed tomography (micro-CT)

After the completion of the 12-day injection regimen, all mice were euthanized using carbon dioxide anesthesia and subsequently underwent immediate systematic morphological, imaging, and pathological evaluations. The skull and soft tissue at bone resorption sites were collected and fixed with 4% paraformaldehyde for 72 hours. Microphotography was employed to capture gross views of skull samples exhibiting bone resorption. Subsequently, micro-CT was performed using a animal scanner at medium resolution with a voxel size of 38.5 μm, voltage of 55 kVp, and a current of 10.9 A. Mineral quantification was performed within 5.0 mm (100 scans) around the cranial suture [39]. NRvecon 1.6 and CTAnv1.13.8.1 were used to analyze bone tissue volume (BV), tissue volume (TV), and bone volume fration (BV/TV) to evaluate the effect of stem cell mitochondrial transfer on bone resorption.

Histological evaluation of the bone resorption

After micro-CT scanning analysis, skull specimens were decalcified in 20% EDTA buffer (pH 7.4) for 7 days. Subsequently, all tissues were embedded in paraffin. Serial skull sections (5 μm) in the sagittal view were stained with hematoxylin&eosin (H&E) or tartrate-resistant acid phosphatase (TRAP) to assess the bone tissue morphology at the bone resorption site. The stained tissue sections were subsequently captured using a pathological microscope. The mean optical density (MOD) values of Trap staining tissue sections were quantitatively analyzed using Image-Pro Plus 6.0 software (Media Cybernetics, USA) [40]. The soft tissues paraffin-embedded sections were stained with rabbit anti-CD68 antibodies or Trap dye (Abcam, USA) [41]. The stained tissue sections were subsequently captured and analyzed as described above.

The analysis were conducted by investigators who were blinded to the treatment groups, ensuring unbiased evaluation.

Inflammatory factors assay

Monocyte-macrophages were activated by stimulating them with LPS derived from Escherichia coli serotype O55:B5 (Solarbio, China) at a concentration of 2 ng/mL. After a 12-hour incubation period, monocyte-macrophages were cultured in a fresh dish and subsequently incubated with or without stem cell-derived mitochondria. All cells were incubated using a cell incubator at 37˚C in a humidified atmosphere of 5% CO_2 [42]. After a 14-day period, the levels of IL-1β and RANKL in the supernatant were assessed using enzyme-linked immunosorbent assay (ELISA) kits (ABclonal, Boston, USA). Absorbance was measured at wavelengths of 450nm and 560nm according to the manufacturer's instructions [43]. The monocyte-macrophages were divided randomly into 4 groups (n = 3/group): Monocyte-macrophages cultured individually as control group (Mac group); Monocyte-macrophages activated by LPS (Mac+LPS group); Monocyte-macrophages co-incubated with mitochondria derived from hSF-MSCs (Mac+Mito group); activated monocyte-macrophages co-incubated with mitochondria derived from hSF-MSCs (Mac+LPS+Mito group).

Detection of osteoclast differentiation

Monocyte-macrophages were induced in osteoclast differentiation medium [DMEM medium containing 25 μg/L M-CSF and 50 μg/L RANKL and incubated with or without stem cell-derived mitochondria, to determine the effect of mitochondria on osteoclast differentiation [44]. The monocyte-macrophages were randomly allocated into 3 groups (n = 3/group): Monocyte-macrophages cultured individually as the control group (Mac group); Monocyte-macrophages induced using RANKL and M-CSF (Mac+RANKL+M-CSF group); Monocyte-macrophages incubated with mitochondria derived from hSF-MSCs and induced using RANKL and M-CSF (Mac+Mito+RANKL+M-CSF group). The osteoclast differentiation phenotype was assessed using the TRAP and methylene blue (MB) staining kit (YJBio, Shanghai, China) according to the manufacturer's protocols. After a 14-day incubation period, the monocyte- macrophages were fixed using a 4% paraformaldehyde solution for a duration of 20 minutes. The plates were rinsed thoroughly with distilled water and stained with TRAP staining solution for 30 minutes or MB staining solution for 15 min [45]. The plates were sealed with glycerol after being rinsed thoroughly with distilled water. Positively stained cells were red and localized in the cytoplasm.

Cell viability Assay

For measurement of monocyte-macrophages proliferation rate, cells were seeded in 96-well plates at a density of 3000 cells/well in DMEM/F-12 medium and cell viability was determined by using a Multiskan FC at days 0, 1, 2, 3, 4, 5, 6, 7, and 8. Cell counting kit-8 (CCK-8) (Beyotime, Beijing, China) solution (10 μL) was added into each well and the cells were continually cultured in the following 4 hours. The viable cell count was measured using the Multiskan FC according to the optical density of formazan pigment at 450 nm [46]. The monocyte-macrophages were divided randomly into 2 groups (n = 6/group): Monocyte-macrophages cultured individually as contral group (Mac group); Monocyte-macrophages co-incubated with hSF-MSCs-derived mitochondria (Mac+Mito group).

For the assessment of mitochondrial function, hSF-MSCs (3×10^6), mitochondria isolated from hSF-MSCs (3×10^6), monocyte-macrophages (3×10^6), and activated monocyte- macrophages (3×10^6) were harvested and the adenosine triphosphate (ATP) was quantified using the CellTiter-Glo® luminescent assay kit (Promega, Wisconsin, USA), while superoxide dismutase (SOD) activity was measured using the SOD activity assay kit (Jonlnbio, Beijing, China), according to the manufacturer's protocols [47, 48]. After a 14-day co-incubation of monocyte-macrophages with mitochondria derived from hSF-MSCs, the ATP and SOD levels of monocyte-macrophages were evaluated using the aforementioned methodology.

For the quantification of intracellular reactive oxygen species (ROS) levels, monocyte-macrophages were incubated in the dark at 37 ℃ for 30 minutes with a ROS-sensitive probe, namely 2',7'-Dichlorodihydrofluorescein diacetate (H2DCFDA), at a concentration of 5 μM. Subsequently, monocyte-macrophages were harvested and suspended in fresh medium [49]. Finally, the ROS levels of the monocyte-macrophages were promptly assessed using FC.

For the assessment of mitochondrial membrane potential (MMP) levels, monocyte-macrophages were incubated with a working solution of 5,5',6,6'-Tetrachloro-1,1',3,3'-tetraethyl-imidacarbocyanine iodide (JC-1) for 20 minutes at 37 ℃ in the dark. Subsequently, the cells were thoroughly washed and resuspended in 300 μL of PBS [50]. Finally, the MMP levels of the monocyte-macrophages were immediately analyzed using FC.

Data analysis and statistics

Statistical analysis was performed using GraphPad Prism software, version 8.02 (GraphPad Software, USA). Statistical significance comparing two groups with parametric data was assessed by two-tailed t-test. Statistical analysis comparing multiple groups with parametric data

was performed by one or two-way ANOVA analysis with Tukey's post hoc test. A value of $P < 0.05$ was considered statistically significant. All data were presented as as mean ± s.d (mean ± standard deviation).

Results

Identification of hSF-MSCs, mitochondria, and exosome

Primary hSF-MSCs have an elongated shape, growing in parallel or spiral arrangements, and forming cell clusters. hSF-MSCs were passaged to the P3 generation, and the cell morphology remained excellent and adhered evenly to the bottom of the culture flask (Figure 1A). The FC analysis revealed that over 95% of hSF-MSCs expressed CD105, CD90, and CD73, while the expression levels of CD19, CD11b, HLA-DR, CD34 and CD45 on hSF-MSCs were below 5% (Figure 1B). Following induced differentiation, hSF-MSCs exhibited the presence of glycosaminoglycans (GAGs), mineralized nodules, and lipid-rich vacuoles (Figure 1C).

The TEM results revealed the presence of mitochondrial-like granules in the extract derived from hSF-MSCs, which had mitochondrial cristae-like structures (Figure 1D). The WB results confirmed that mitochondrial specific membrane protein TOMM22 was existing in the precipitation (Figure 1E). The fluorescence signals captured by laser confocal microscopy revealed the co-localization of Mitotracker Green-labeled mitochondria within monocyte-macrophages labeled with Dil liposomes (Figure 1I).

The TEM results revealed the presence of circular particles in the extract obtained from the culture supernatant of hSF-MSCs, exhibiting a size resembling exosomes, approximately 50 nm in diameter (Figure 1F). The particle size distribution in the extract, as determined by NTA analysis, predominantly ranged from approximately 30 to 200 nm (Figure 1G). The FC analysis revealed that more than 99% of particles in the extract exhibited expression of CD63, a surface antigen specific to exosomes (Figure 1H).

Gross view and micro-CT analysis of skulls

The gross view of the skulls revealed more prominent mineralized plaques in the mice from the MSCs, Mito, and Exo groups compared with that in PBS group. In comparison to the Mito group, both the MSCs group and Exo group exhibited no significant differences (Figure 2A). The three-dimensional (3D) imaging of skulls revealed that the PBS group exhibited more pronounced bone resorption compared to the other groups (Figure 2B).

The PBS group exhibited a slightly higher bone tissue volume (BV) compared to the NC group, as revealed by micro-CT analysis ($p \leq 0.05$, Table 1; Figure 2C). However, the TV of the PBS group exhibited a significant increase compared to that of the NC groups ($p \leq 0.001$,

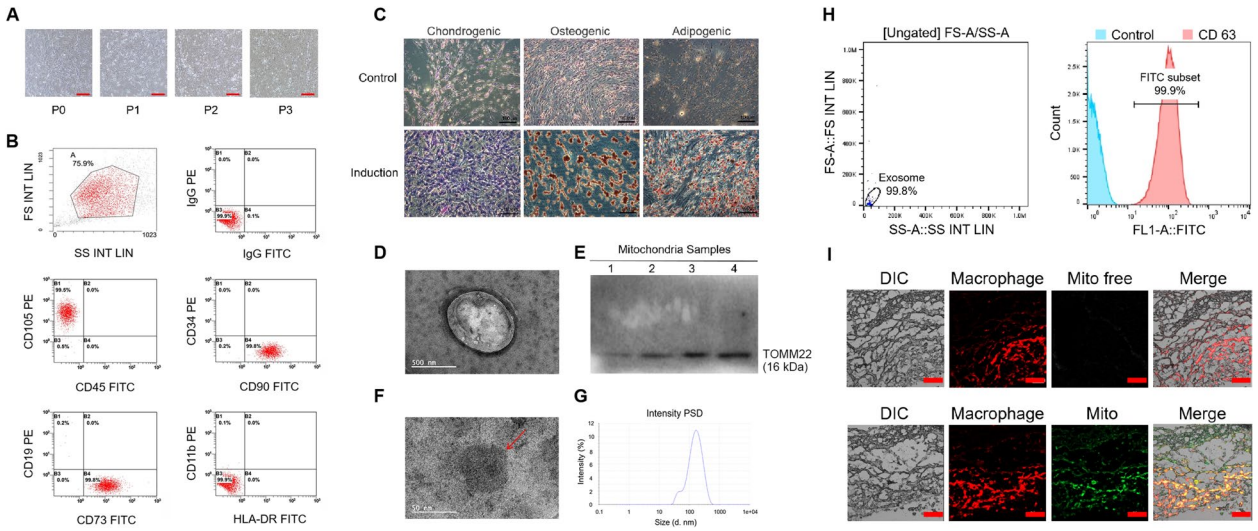

Fig. 1 Identification of hSF-MSCs, mitochondria, and exosome. (**A**) Morphological observation of hSF-MSCs, Scale bar = 200 μm. (**B**) FC analysis of surface markers on hSF-MSCs. (**C**) Chemical staining of hSF-MSCs after chondrogenic, osteogenic, and adipogenic differentiation, Scale bars = 100 μm (chondrogenic-TB staining, osteogenic-alizarin red staining, adipogenic-oil red O staining). (**D**) The morphology of mitochondria under TEM, Scale bar = 500 nm. (**E**) The WB results of TOMM22 (the numbers 1 to 4 correspond to four mitochondrial samples). (**F**) The morphology of exosome under TEM, Scale bar = 50 nm. (**G**) The NTA results of exosomes. (**H**) FC analysis of surface marker (CD63) on exosomes. (**I**) The tracing result of hSF-MSCs-derived mitochondria in vivo, Scale bars = 100 μm. Macrophage, Monocyte-macrophages labeled with Dil liposomes; Mito, Mitotracker Green-labeled hSF-MSCs-derived mitochondria; Mito free, Mito injection was not administered; PSD, Particle size distribution

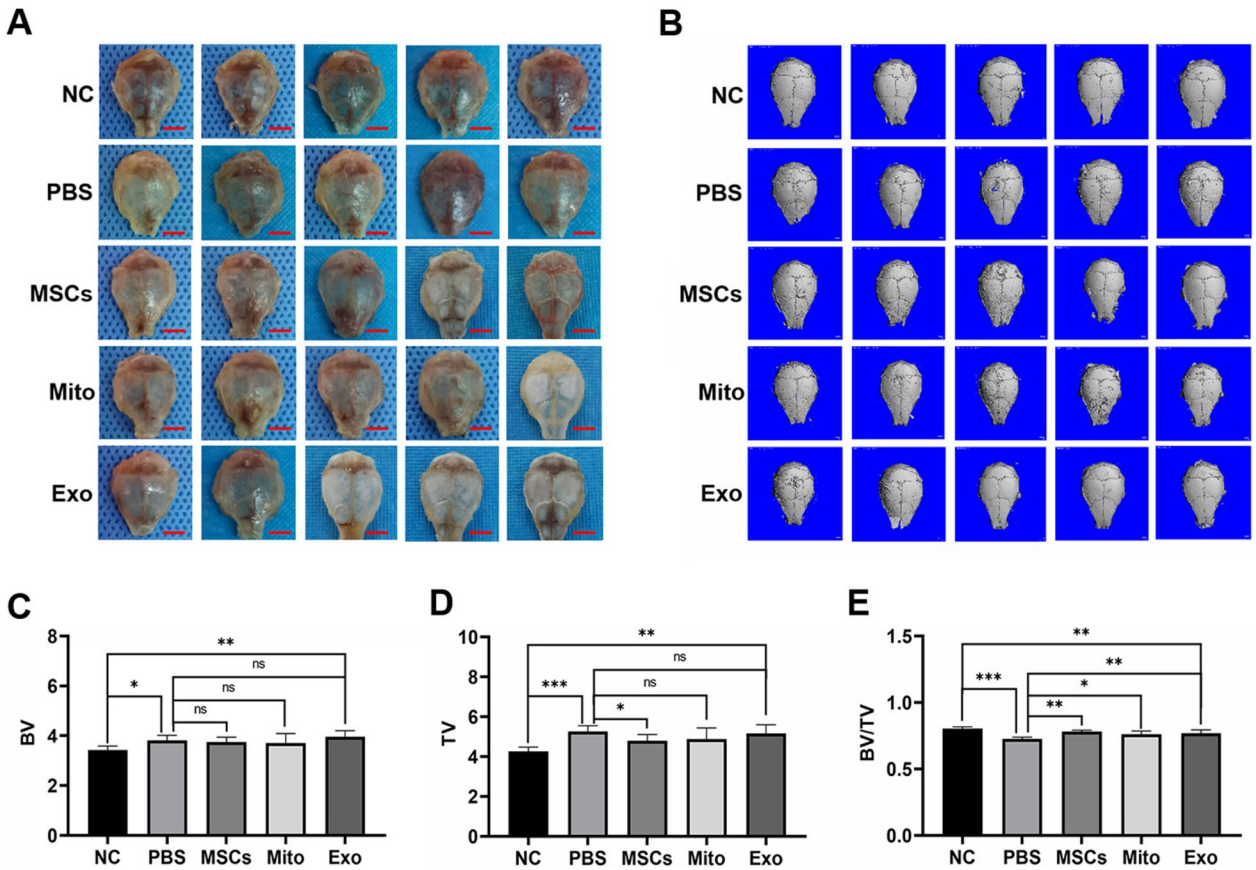

Fig. 2 Gross view and micro-CT analysis of skulls ($n = 5$/group). (**A**) Gross view of bone resorption in mice skull, Scale bar = 5 mm. (**B**) 3D image of skulls. (**C**) Micro-CT analysis of the BV. (D) Micro-CT analysis of the TV. (E) Micro-CT analysis of the BV/TV. Exo, exosome group; Mito, mitochondria group; MSCs, hSF-MSCs group; NC, normal control group; ns, no significance; PBS, negative control group; *$p < 0.05$; **$p < 0.01$; ***$p < 0.001$

Table 1 Micro-CT analysis of skulls

Groups	BV (AV ± SD)	TV (AV ± SD)	BV/TV (AV ± SD)
NC	3.4239 ± 0.1622	4.2550 ± 0.2195	0.8049 ± 0.0115
PBS	3.8130 ± 0.2026	5.2564 ± 0.2892	0.7256 ± 0.0143
MSCs	3.7401 ± 0.2017	4.7953 ± 0.3048	0.7804 ± 0.0114
Mito	3.7103 ± 0.3827	4.8767 ± 0.5616	0.7619 ± 0.0238
Exo	3.9640 ± 0.2402	5.1587 ± 0.4346	0.7697 ± 0.0242

Note: The bone volume fration (BV/TV) represents the ratio of bone tissue volume (BV) to tissue volume (TV), which directly reflects the change of bone mass. *Abbreviations*: *AV* average value, *SD* standard deviation

Table 1; Figure 2D). The BV and TV of the Mito group exhibited similarity to that of the MSCs and Exo groups ($p > 0.05$, Table 1; Figure 2C,D). The BV/TV of the PBS group was found to be significantly lower compared to the other groups ($p \leq 0.05$, Table 1; Figure 2E). However, the BV/TV of the MSCs, Mito and Exo groups were lower than that of the NC group ($p < 0.05$, Table 1; Figure 2E). Additionally, there were no statistically significant differences in the BV/TV observed among the MSCs, Mito, and Exo groups ($p > 0.05$, Table 1; Figure 2E).

Histological assessment of skulls and periostea

Bone resorption was mainly found at the middle cranial suture of mice (Figure 3A). Trap staining of skulls revealed a significantly higher osteoclast surface area and an increased number of TRAP-positive osteoclasts in the PBS group compared to those in the NC, MSCs, Mito, and Exo groups ($p \leq 0.01$, Figure 3A,B,F). The histological evaluation of periostea revealed that the levels of CD68 and TRAP staining were higher in the PBS group compared to the NC, MSCs, Mito, and Exo groups ($p \leq 0.001$, Figure 3A,C,D). The PBS group exhibited more prominent bone resorption and wider midcranial suture, as evidenced by the H&E staining, in comparison to the NC, MSCs, Mito, and Exo groups ($p \leq 0.01$, Figure 3A,E). In addition, the immunohistochemical results of the Mito group did not exhibit significant differences compared to those of the MSCs and Exo groups ($p > 0.05$, Figure 3C-F).

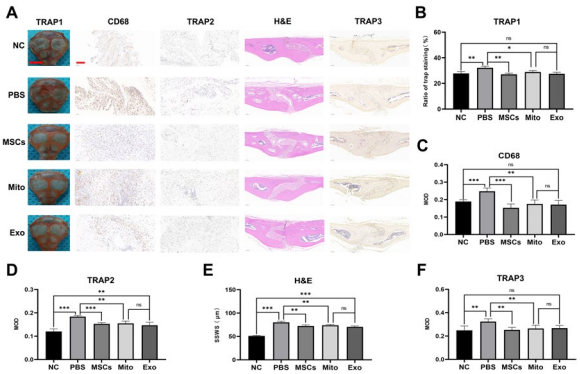

Fig. 3 Histological analysis of femurs ($n = 5$/group). (**A**) Immunohistochemical staining of skulls and periostea, Scale bar of skulls = 5 mm, Scale bar of tissue sections = 100 μm. (**B**) Image J analysis of overall TRAP staining in skulls. (**C**) Image J analysis of CD68 stained periosteum sections. (**D**) Quantitative analysis of TRAP-stained periosteum sections using Image J. (**E**) Quantitative analysis of H&E stained skull sections using Image J. (F) Image J analysis of TRAP-stained skull sections. CD68, CD68 staining in periostea of skulls; Exo, Exosome group; H&E, H&E staining in skulls; Mito, Mitochondria group; MSCs, hSF-MSCs group; NC, Normal control group; ns, no significance; PBS, Negative control group; SSWS, the sagittal suture width of the skulls; TRAP1, TRAP staining of the gross skulls; TRAP2, TRAP staining of the periostea; TRAP3, TRAP staining of the skull sections; *$p < 0.05$; **$p < 0.01$; ***$p < 0.001$

The biological behavior of monocyte-macrophage

Mito Tracker Green-labeled mitochondria were observed in Mito Tracker Deep Red-labeled monocyte-macrophages (Figure 4A). The Mac+Mito+RANKL+M-CSF group showed inconspicuous red in the cytoplasm and less cell fusion activity compared to Mac+RANKL+M-CSF group (Figure 4B,C).

The production of SOD is a prevalent phenomenon observed in hSF-MSCs, Mito, Mac, and activated Mac. The levels of SOD were significantly higher in hSF-MSCs and Mito, compared to Mac. Additionally, activated Mac exhibited lowest SOD levels ($p \leq 0.05$, Figure 4D). After a 14-day co-incubation process, the Mac+Mito group and Mac+LPS+Mito group demonstrated elevated levels of SOD and reduced levels of ROS compared to the Mac group and Mac+LPS group ($p \leq 0.01$, Figure 4E,F). The Mac+Mito group and Mac+LPS+Mito group demonstrated decreased concentrations of RANKL and IL-1β in comparison to the groups without Mito co-incubation ($p \leq 0.05$, Figure 4G).

The generation of ATP is a widespread occurrence observed in hSF-MSCs, Mito, Mac, and activated Mac. The levels of ATP exhibited a marked increase specifically in activated Mac and hSF-MSCs ($p \leq 0.05$, Figure 4H). After a 14-day co-incubation process, the Mac group,

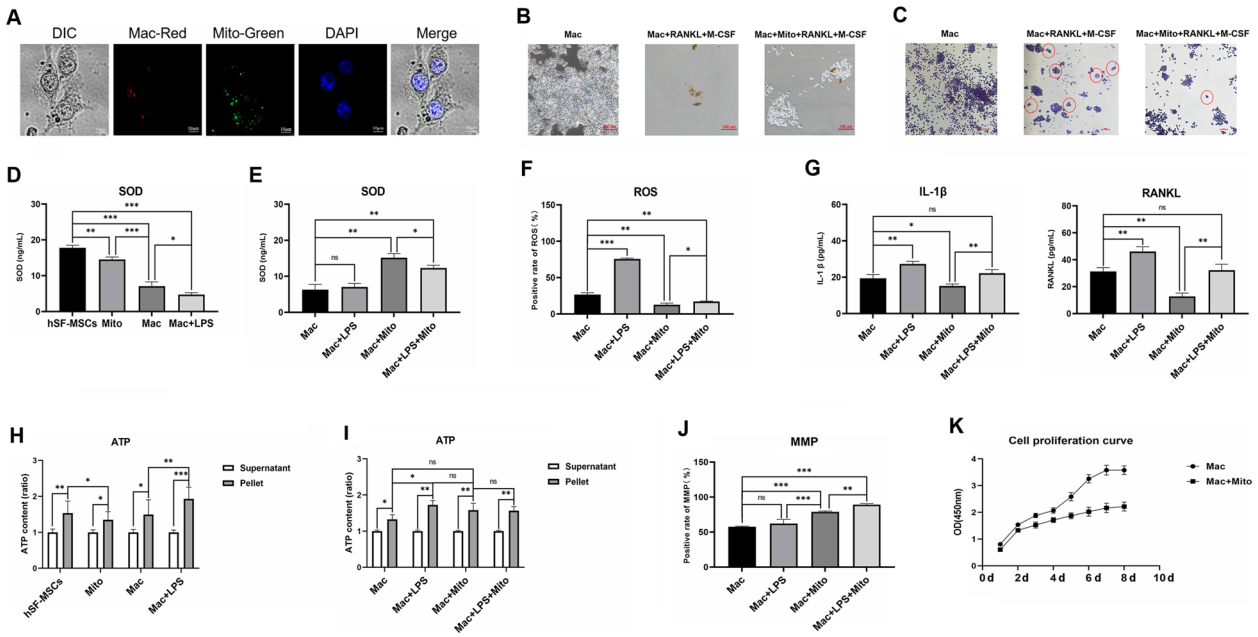

Fig. 4 The impact of mitochondria derived from hSF-MSCs on monocyte-macrophage function. (**A**) The tracing result of mitochondria *in vitro*, Scale bars = 10 μm. (**B**) Revealing osteoclast differentiation via TRAP staining, Scale bars = 100 μm. (**C**) Revealing cell fusion via MB staining, Scale bars = 100 μm. (**D**) The levels of SOD in hSF-MSCs, Mito, Mac, and activated Mac. (**E**) The levels of SOD in Mac following co-incubation process. (**F**) The levels of ROS in Mac after co-incubation process. (**G**) The levels of IL-1β and RANKL in the supernatant derived from Mac. (**H**) The levels of ATP in hSF-MSCs, Mito, Mac, and activated Mac. (**I**) The levels of ATP in Mac following co-incubation process. (**J**) The levels of MMP in Mac. (**K**) Viability assessment of Mac. Mac, Monocyte-macrophages; Mac+LPS, Reactive monocyte-macrophages stimulated by LPS (2 ng/mL); Mac-Red, Mac labeled with Mito tracker Deep Red; Mito, Mitochondria derived from hSF-MSCs; Mito-Green, Mito labeled with Mito tracker Green; ns, no significance; *$p < 0.05$; **$p < 0.01$; ***$p < 0.001$

Mac+Mito group, and Mac+LPS+Mito group exhibited comparable levels of ATP . The Mac+LPS group displayed elevated ATP levels compared to the Mac group ($p \leq 0.01$, Figure 4I). The MMP levels of the Mac+Mito group and Mac+LPS+Mito group were found to be significantly higher compared to those of the Mac group and Mac+LPS group ($p \leq 0.001$, Figure 4J). During co-incubation process, the Mac+Mito group showed a weaker cell proliferation than the Mac group (Figure 4K).

Discussion

In the present study, we discovered that mitochondria derived from hSF-MSCs exhibit the capacity to transfer into monocyte-macrophages and effectively suppress their biological behavior both in vivo and in vitro, thereby exerting a significant inhibitory impact on inflammatory bone resorption.

MSCs-based therapy exhibits significant potential in tissue regeneration and modulation of inflammatory responses [51]. In order to address the issue of inflammatory bone resorption, research attention has been redirected towards the investigation of stem cells. Inflammatory bone resorption is a significant adverse factor leading to the failure of fracture healing and shaping [52, 53]. Inflammatory bone resorption have a close connection to osteoclast differentiation and maturation. Osteoclasts attached to fracture site could be activated by inflammatory cytokines, such as TNF-α, IL-1β, RANKL, M-CSF, etc [54, 55]. Therefore, inhibiting the secretion of inflammatory cells may be an effective way to avoid inflammatory bone resorption. Multiple studies have demonstrated the capacity of stem cells to modulate the biological behaviors of inflammatory cells through mitochondrial transfer, encompassing proliferation, phagocytosis, secretion, and other processes [56, 57]. Fortunately, our aforementioned findings once again substantiate the robustness of the previous theoretical framework and the current trajectory of investigation. MSCs could yield mitochondrial transfer to monocyte-macrophages and inhibit cell proliferation and secretion of inflammatory factors [58]. To advance the investigation of stem cell-derived mitochondrial transfer for inhibiting inflammatory bone resorption, a reliable source of mitochondria is imperative. In this regard, hSF-MSCs, characterized by their robust proliferation capacity and stable phenotype, exhibit potential as mitochondrial donor cells. Our results revealed that the mitochondrial morphology and structure extracted from hSF-MSCs were well maintained and the expression of mitochondrial membrane proteins was characteristic, so that the experiment could be carried out smoothly relying on hSF-MSCs. Meanwhile, the mitochondria derived from hSF-MSCs could be transferred into monocyte-macrophages in the bone resorption mice model, which is essential for the regulation of cellular biological behavior. In conclusion, the aforementioned findings suggest that mitochondria derived from hSF-MSCs may exert a regulatory role in suppressing inflammatory bone resorption.

Local injection of stem cell-derived mitochondria has demonstrated significant therapeutic potential in tissue repair, as evidenced by comprehensive investigations conducted in the fields of respiratory, nervous, circulatory, and motor systems [59–61]. The present studies show that MSCs immunoregulatory effect on inflammatory cells relies also on mitochondrial transfer, but the role of stem cell-derived mitochondria on inflammatory cells remains unclear [62]. In this study, the immunohistochemistry results revealed a reduction in CD68+ cell infiltration in the mitochondria injection group, indicating that the proliferation of monocyte-macrophages (CD68+) was inhibited by mitochondria derived from hSF-MSCs. In addition, the relative bone volume of the mitochondria injection group was found to be significantly higher compared to that of the negative control group, indicating a reduced formation of bone resorption attribute to mitochondria derived from hSF-MSCs. However, the mineralization levels of the mitochondria injection group have not been restored to normal levels. Therefore, it can be hypothesized that the repression of monocyte-macrophage proliferation mediated by mitochondrial injection alleviates inflammatory bone resorption. Summarizing the results of H&E and TRAP staining, it was observed that the skull bone resorption and osteoclast count in the mitochondria injection group were more pronounced compared to the normal control group, yet less severe than those in the negative control group. Thus, histochemical staining indicated that mitochondria injection significantly reduced the number of infiltrated mature osteoclasts at the bone resorption site and effectively inhibited inflammatory bone resorption in vivo. In conclusion, the aforementioned findings indicate that the inhibition of inflammatory bone resorption in mice can be attributed to the suppression of monocyte-macrophage proliferation and osteoclast activity via mitochondrial transfer from hSF-MSCs.

Stem cell-derived mitochondria could be transferred and integrated into the mitochondrial network of host cells in vitro, which could improve the impaired mitochondrial function and maintain the level of oxidative stress [63]. Additionally, it has been observed that MSCs possess the ability to attenuate macrophage secretion, potentially contributing to the reduction of bone resorption [64]. In this study, the phenomenon of mitochondrial transfer was observed during co-incubation of mitochondria derived from hSF-MSCs with monocyte-macrophages. Meanwhile, mitochondria derived from

hSF-MSCs exhibited the ability to suppress the production of RANKL and IL-1β by monocyte-macrophages, which was associated with osteoclast differentiation. According to the results of TRAP and MB staining targeting monocyte-macrophages, mitochondria derived from hSF-MSCs could effectively suppress cell fusion, thereby inevitably inhibiting osteoclastogenesis. Therefore, hSF-MSCs-derived mitochondrial transfer may exert an active role in the inhibition of bone resorption through the regulation of osteoclast differentiation and maturation. According to the available studies, osteoclasts derived from monocyte-macrophages undergo cytoskeletal deformation regulated by ROS, and mitochondria play a pivotal role in this process by efficiently eliminating ROS through the utilization of self-synthesized SOD [65, 66]. The ELISA results of this study demonstrated that mitochondria derived from hSF-MSCs possess the capability to produce SOD and effectively enhance the levels of SOD in monocyte-macrophages. Moreover, the FC assay demonstrated that mitochondria derived from hSF-MSCs possess the ability to attenuate levels of ROS in monocyte-macrophages. Therefore, based on the aforementioned findings, it can be inferred that mitochondria derived from hSF-MSCs modulate ROS levels in monocyte-macrophages through the synthesis of SOD, consequently influencing osteoclastogenesis and inflammatory bone resorption. In conclusion, the inhibitory effect of mitochondria derived from hSF-MSCs on inflammatory bone resorption is likely mediated through the regulation of inflammatory factor secretion, modulation of osteoclast differentiation, and reduction of oxidative stress levels in monocyte-macrophages.

Previous studies have presented substantial evidence supporting the ability of stem cell mitochondrial transfer to modulate host cell mitochondrial function, influence energy metabolism and MMP, subsequently impacting the biological behavior of host cells [67, 68]. In this study, the ATP detection results indicated that activated monocyte-macrophages exhibited an enhanced level of ATP synthesis, while mitochondria derived from hSF-MSCs demonstrated the capacity for ATP synthesis. However, the transfer of hSF-MSCs-derived mitochondria to monocyte-macrophages did not significantly affect their energy metabolism levels. Additionally, the FC assay demonstrated that mitochondria derived from hSF-MSCs actively contributed to the maintenance of MMP in monocyte-macrophages, thereby potentially exerting a pivotal role in attenuating ROS production. The CCK-8 assay revealed that mitochondria derived from hSF-MSCs possess the capability to inhibit the proliferation of monocyte-macrophages, suggesting their potential in mitigating inflammatory bone resorption. Therefore, it is demonstrated that mitochondria derived from hSF-MSCs can maintain the MMP in monocyte-macrophages while inhibiting their proliferation; however, the levels of ATP synthesis in these cells remain largely unaffected. In conclusion, it can be inferred that the inhibitory effect of mitochondria derived from hSF-MSCs on inflammatory bone resorption can be attributed to their modulation of MMP levels in monocyte-macrophages and the suppression of monocyte-macrophage proliferation, rather than to their impact on energy metabolism.

The present findings are consistent with previous reports that have demonstrated the inhibitory effects of MSCs on inflammatory cells [69, 70]. However, it is crucial to fully appreciate the inherent variability between internal and external environments, including but not limited to the impact of oxygen content on cellular levels of ROS, the in vivo role of periosteal stem cells, disparities in biomechanical milieu, as well as variations in the rate of decomposition for pro-inflammatory substances within internal and external settings. The aforementioned factors necessitate comprehensive exploration, while the intricate inflammatory microenvironment encompasses diverse cellular constituents in vivo. Therefore, we primarily rely on the experimental results obtained in vivo to substantiate our findings. Based on the aforementioned research findings, our study is the first article that employs stem cell-derived mitochondria to address the issue of inflammatory bone resorption, thereby providing a theoretical foundation for the clinical application of localized stem cell injection as a therapeutic approach to address inflammatory bone resorption. However, it is imperative to acknowledge the inherent limitations of this article. Firstly, the sustained viability of purified stem cell-derived mitochondria in vitro is notably limited, thereby imposing significant constraints on the clinical trials and applicability of stem cell-derived mitochondria. Secondly, it is imperative to augment funding investment in the advancement of mitochondrial preservation solutions or refine clinical therapeutic platforms in order to efficiently minimize the duration required for isolation and transportation of mitochondria from stem cell. Thirdly, it is noteworthy that the outer membrane of these mitochondria is seldom directly stimulated by exogenous stimuli, but the immunogenicity of mitochondria derived from stem cells remains uncertain in comparison to that of the stem cells themselves.

The treatment of inflammatory bone resorption via local injection of stem cell-derived mitochondria has not yet been clinically validated and faces numerous potential challenges. However, the experimental results from this study demonstrate that stem cell-derived mitochondria hold significant potential for treating inflammatory bone resorption, providing a crucial theoretical foundation for the future clinical application of this therapeutic

approach. Therefore, based on the findings of this study, we can cautiously and optimistically propose that clinical researchers may develop a novel therapy for inflammatory bone resorption utilizing stem cell mitochondrial transfer technology.

Conclusions

Our study demonstrated the successful transfer of stem cell-derived mitochondria into monocyte-macrophages, resulting in an inhibitory effect on cell vitality and inflammatory bone resorption. These findings suggest that stem cells may exert a beneficial effect on bone resorption inhibition through the transfer of mitochondria. In summary, the utilization of stem cell-derived mitochondria presents a promising strategy for attenuating inflammatory bone resorption.

Abbreviations

BV/TV	Bone volume/Tissue volume, relative bone volume
BMSCs	Bone marrow-derived mesenchymal stem cells
CCK-8	Cell Counting Kit-8
ELISA	Enzyme Linked Immunosorbent Assay
Exo	exosome
hSF	human synovial fluid
hSF-MSCs	human synovial fluid-derived mesenchymal stem cells
H&E	hematoxylin&eosin
LPS	lipopolysaccharide
Micro-CT	Micro-computed tomography
Mito	mitochondria
MSCs	Mesechymal stem cells
M-CSF	Macrophage-colony stimulating factor
RANKL	Receptor Activator of Nuclear Factor-κB Ligand
TB	toluidine blue
TOMM22	Translocase Of Outer Mitochondrial Membrane 22
Trap	Tartrate resistant acid phosphatase

Acknowledgements

The authors would like to express their gratitude to all the investigators from the Graduate School of Peking University who participated in this project.

Clinical trial number

Not applicable.

Authors' contributions

X.L. designed the study, performed the experiments, analyzed the data and drafted the manuscript. J.S. collected data. X.L. reviewed the manuscript. W.L. supervised the project. Z.D. designed the study and revised the manuscript. All authors have read and approved the final manuscript.

Funding

This work was supported by the National Natural Science Foundation of China (82072515 to WL), Guangdong Basic and Applied Basic Research Foundation (2023A1515220072 to ZD) and Shenzhen Science and Technology Projects (JCYJ20220530150615035 to XL).

Data availability

The datasets used and/or analysed during the current study are available from the corresponding author on reasonable request.

Declarations

Ethics approval and consent to participate

The cell experiment conducted in this study was approved by the Ethics Committee of Shenzhen Second People's Hospital(No. 2024-102-01PJ), and the joint fluid samples were collected with the informed consent of all participants. The animal experiment received approval from the Ethics Committee of Peking University Graduate School(No. ER-0023-042) and performed in accordance with the national guidelines for animal welfare.

Consent for publication

Not applicable.

Competing interests

The authors declare no competing interests.

Author details

[1]Department of Orthopedics, Shenzhen Second People's Hospital, The First Affiliated Hospital of Shenzhen University, Health Science Center), Shenzhen 518035, Guangdong, China. [2]Guangdong Key Laboratory for Biomedical Measurements and Ultrasound Imaging, National-Regional Key Technology Engineering Laboratory for Medical Ultrasound, School of Biomedical Engineering, Shenzhen University Medical School, Shenzhen 518060, Guangdong, China. [3]Department of Orthopedics, The First Affiliated Hospital of Wenzhou Medical University, Wenzhou 325005, Zhejiang, China. [4]Geriatrics Center, The First Affiliated Hospital of Wenzhou Medical University, Wenzhou 325005, Zhejiang, China. [5]Department of Orthopedics, Heilongjiang Provincial Hospital, Harbin 150036, Heilongjiang, China.

Received: 23 November 2024 Accepted: 12 March 2025
Published online: 22 March 2025

References

1. Schini M, Vilaca T, Gossiel F, Salam S, Eastell R. Bone turnover markers: basic biology to clinical applications. Endocr Rev. 2023;44(3):417–73.
2. Song S, Guo Y, Yang Y, Dehao Fu. Advances in pathogenesis and therapeutic strategies for osteoporosis. Pharmacol Ther. 2022;237:108168.
3. Wu Z, Yuan K, Zhang Q, Guo JJ, Yang H, Zhou F. Antioxidant PDA-PEG nanoparticles alleviate early osteoarthritis by inhibiting osteoclastogenesis and angiogenesis in subchondral bone. J Nanobiotechnol. 2022;20(1):479.
4. Tian L, Sheng Y, Huang L, Chow DHK, Chau WH, Tang N, Ngai T, Wu C, Lu J, Qin L. An innovative Mg/Ti hybrid fixation system developed for fracture fixation and healing enhancement at load-bearing skeletal site. Biomaterials. 2018;180(10):173–83.
5. Romeo SG, Alawi KM, Rodrigues J, Singh A, Kusumbe AP, Ramasamy SK. Endothelial proteolytic activity and interaction with non-resorbing osteoclasts mediate bone elongation. Nat Cell Biol. 2019;21(4):430–41.
6. Lazarov T, Juarez-Carre S, Cox N, Geissmann F. Physiology and diseases of tissue-resident macrophages. Nature. 2023;618(7966):698–707.
7. McDonald MM, Khoo WH, Ng PY, Xiao Y, Zamerli J, Thatcher P. Osteoclasts recycle via osteomorphs during RANKL- stimulated bone resorption. Cell. 2021;184(7):1940.
8. Wang L-T, Chen L-R, Chen K-H. Hormone-related and drug-induced osteoporosis: a cellular and molecular overview. Int J Mol Sci. 2023;24(6):5814.
9. Wang Lu, Li Y, Moyan Xu, Deng Z, Zhao Y, Yang M. Regulation of inflammatory cytokine storms by mesenchymal stem cells. Front Immunol. 2021;12:726909.
10. Maedeh A, Amene S, Nima R. Anti-inflammatory and M2 macrophage polarization-promoting effect of mesenchymal stem cell- derived exosomes. Int Immunopharmacol. 2021;97: 107823.
11. Zhang ZY, Huang SS, Wu SF, Qi JJ, Li WC, Liu SS. Clearance of apoptotic cells by mesenchymal stem cells contributes to immunosuppression via PGE2. EBioMedicine. 2019;45:341–50.
12. Velarde F, Ezquerra S, Delbruyere X, Caicedo A, Hidalgo Y, Khoury M. Mesenchymal stem cell-mediated transfer of mitochondria: mechanisms and functional impact. Cell Mol Life Sci. 2022;79(3):1–20.
13. Yuan Y, Yuan L, Li L, Liu F, Liu J, Chen Y. Mitochondrial transfer from mesenchymal stem cells to macrophages restricts inflammation and alleviates kidney injury in diabetic nephropathy mice via PGC-1α activation. Stem Cells. 2021;39(7):913–28.

14. Bing W, Mingliang Ji, Yucheng L, Shanzheng W, Yuxi L, Rui G. Mitochondrial transfer from bone mesenchymal stem cells protects against tendinopathy both in vitro and in vivo. Stem Cell Res Ther. 2023;14(1):104.
15. Xia L, Zhang C, Lv N, Liang Z, Ma T, Cheng H. AdMSC-derived exosomes alleviate acute lung injury via transferring mitochondrial component to improve homeostasis of alveolar macrophages. Theranostics. 2022;12(6):2928–47.
16. Hayes KN, Giannakeas V, Wong AK. Bisphosphonate use is protective of radiographic knee osteoarthritis progression among those with low disease severity and being non-overweight: data from the osteoarthritis initiative. J Bone Miner Res. 2020;35(12):2318–26.
17. Giner M, Rios J, Montoya J, Vázquez A, Miranda C, Pérez-Cano R. Alendronate and raloxifene affect the osteoprotegerin/ RANKL system in human osteoblast primary cultures from patients with osteoporosis and osteoarthritis. Eur J Pharmacol. 2011;650(2–3):682–7.
18. Li Y, Ju XJ, Fu H, Zhou CH, Gao Y, Wang J. Composite separable microneedles for transdermal delivery and controlled release of salmon calcitonin for osteoporosis. ACS Appl Mater Interfaces. 2022;15(1):638–50.
19. Iantomasi T, Romagnoli C, Palmini G, Donati S, Falsetti I, Miglietta F. Oxidative stress and inflammation in osteoporosis: molecular mechanisms involved and the relationship with microRNAs. Int J Mol Sci. 2023;24(4): 3772.
20. Terashima A, Takayanagi H. The role of bone cells in immune regulation during the course of infection. Semin Immunopathol. 2019;41(5):619–26.
21. Zeytin IC, Alkan B, Ozdemir C, Cetinkaya DU, Okur FV. Alterations in hematopoietic and mesenchymal stromal cell components of the osteopetrotic bone marrow niche. Stem Cells Transl Med. 2022;11(3):310–21.
22. Orit S, Shifra H, Shani A-P, Keren G, Luba E-B, Asaf W. CX3CR1hi monocyte/macrophages support bacterial survival and experimental infection-driven bone resorption. J Infect Dis. 2016;213(9):1505–15.
23. Ishii T, Pera RAR, Greely HT. Ethical and legal issues arising in research on inducing human germ cells from pluripotent stem cells. Cell Stem Cell. 2013;13(2):145–8.
24. Rosner M, Horer S, Feichtinger M, Hengstschl M. Multipotent fetal stem cells in reproductive biology research. Stem Cell Res Ther. 2023;14(1):157.
25. Liu D, Gao Y, Liu J, Huang Y, Yin J, Feng Y. Intercellular mitochondrial transfer as a means of tissue revitalization. Signal Transduct Target Ther. 2021;6(1):65.
26. Xiao Xu, Limei Xu, Xia J, et al. Harnessing knee joint resident mesenchymal stem cells in cartilage tissue engineering. Acta Biomater. 2023;168:372–87.
27. Furuoka H, Endo K, Sekiya I. Mesenchymal stem cells in synovial fluid increase in number in response to synovitis and display more tissue-reparative phenotypes in osteoarthritis. Stem Cell Res Ther. 2023;14(1):244.
28. Yuan L, Zhao Na, Wang J, Liu Y, Meng Li, Guo S. Major vault protein (MVP) negatively regulates osteoclastogenesis via calcineurin-NFATc1 pathway inhibition. Theranostics. 2021;11(15):7247–61.
29. Jia Z, Wang S, Liu Q. Identification of differentially expressed genes by single-cell transcriptional profiling of umbilical cord and synovial fluid mesenchymal stem cells. J Cell Mol Med. 2020;24(2):1945–57.
30. Hua Q, Zhang Y, Li H, Li H, Jin R, Li Li. Human umbilical cord blood-derived MSCs trans-differentiate into endometrial cells and regulate Th17/Treg balance through NF-κB signaling in rabbit intrauterine adhesions endometrium. Stem Cell Res Ther. 2022;13(1):1–15.
31. Libo Yu, Xie M, Zhang F, Wan C, Yao X. TM9SF4 is a novel regulator in lineage commitment of bone marrow mesenchymal stem cells to either osteoblasts or adipocyte. Stem Cell Res Ther. 2021;12(1):1–16.
32. Rahman MH, Xiao Q, Zhao S, Wei A-C, Ho Y-P. Extraction of functional mitochondria based on membrane stiffness. Methods Mol Biol. 2021;2276:343–55.
33. Jiao H, Jiang D, Xiaoyu Hu, Wanqing Du, Ji L, Yang Y. Mitocytosis, a migrasome-mediated mitochondrial quality-control process. Cell. 2021;184(11):2896–910.
34. Liu Y, Zhang H, Liu Y, Zhang S, Su P, Wang L. Hypoxia-induced GPCPD1 depalmitoylation triggers mitophagy via regulating PRKN-mediated ubiquitination of VDAC1. Autophagy. 2023;19(9):1–21.
35. Liang Y, Xiao Xu, Li X. Chondrocyte-targeted MicroRNA delivery by engineered exosomes toward a cell-free osteoarthritis therapy. ACS Appl Mater Interfaces. 2020;12(33):36938–47.
36. Xiao Xu, Liang Y, Li X. Exosome-mediated delivery of kartogenin for chondrogenesis of synovial fluid-derived mesenchymal stem cells and cartilage regeneration. Biomaterials. 2021;269:120539.
37. Jin H, Liu Y, Liu X, Khodeiry MM, Lee JK, Lee RK. Hematogenous macrophages contribute to fibrotic scar formation after optic nerve crush. Mol Neurobiol. 2022;59(12):7393–403.
38. O'Brien CG, Ozen MO, Ikeda G. Mitochondria-rich extracellular vesicles rescue patient-specific cardiomyocytes from doxorubicin injury: insights into the SENECA trial. JACC Cardio Oncol. 2021;3(3):428–40.
39. Zhenglin Z, Yi C, Jing Z, Gao Shengqiang Wu, Dandong LX. Lactate mediates the bone anabolic effect of high-intensity interval training by inducing osteoblast differentiation. J Bone Joint Surg Am. 2023;105(5):369–79.
40. Yajun Li, Qi Z, Lihong T, Kai Z, Shuangshuang C, Yunshang Y. Urolithin B suppressed osteoclast activation and reduced bone loss of osteoporosis via inhibiting ERK/NF-κB pathway. Cell Prolif. 2022;55(10):e13291.
41. Kang H-J, Park S-S, Tripathi G, Lee B-T. Injectable demineralized bone matrix particles and their hydrogel bone grafts loaded with β-tricalcium phosphate powder and granules: a comparative study. Materials Today Bio. 2022;16: 100422.
42. Fukatsu M, Ohkawara H, Wang X, Alkebsi L, Furukawa M, Mori H. The suppressive effects of Mer inhibition on inflammatory responses in the pathogenesis of LPS-induced ALI/ARDS. Sci Signal. 2022;15(724):eabd2533.
43. Wei L, Chen W, Huang L, Wang H, Yuangang Su, Liang J. Alpinetin ameliorates bone loss in LPS-induced inflammation osteolysis via ROS mediated P38/PI3K signaling pathway. Pharmacol Res. 2022;184:106400.
44. Yang Y, Liu Z, Jinzhi Wu, Bao S, Wang Y, Li J. Nrf2 Mitigates RANKL and M-CSF induced osteoclast differentiation via ROS-dependent mechanisms. Antioxidants (Basel). 2023;12(12):2094.
45. Yang-Lin Wu, Zhang CH, Teng Y, Pan Y, Liu NC, Liu PX. Propionate and butyrate attenuate macrophage pyroptosis and osteoclastogenesis induced by CoCrMo alloy particles. Mil Med Res. 2022;9(1):46.
46. Jun Su, Li Y, Liu Q, Peng G, Qin C, Li Y. Identification of SSBP1 as a ferroptosis-related biomarker of glioblastoma based on a novel mitochondria-related gene risk model and in vitro experiments. J Transl Med. 2022;20(1):440.
47. Hou Q, Yan F, Li X, Liu H, Yang X, Dong X. ATP5me alleviates high glucose-induced myocardial cell injury. Int Immunopharmacol. 2024;129: 111626.
48. Cheng JJ, Ma XD, Ai GX, Qiu-Xia Yu, Chen XY, Yan F, Li YC, Xie JH, Zi-Ren Su, Xie QF. Palmatine protects against MSU-induced gouty arthritis via regulating the NF-κB/NLRP3 and Nrf2 pathways. Drug Des Devel Ther. 2022;16:2119–32.
49. Kuběnová L, Haberland J, Dvořák P, Šamaj J, Ovečka M. Spatiotemporal distribution of reactive oxygen species production, delivery, and use in Arabidopsis root hairs. Plant Physiol. 2023;193(4):2337–60.
50. Ai W, Yingcui Bu, Huang H, Wang J, Mengjuan Ren Yu, Deng YZ, Wang S, Zhi-Peng Yu, Zhou H. Bifunctional single-molecular fluorescent probe: visual detection of mitochondrial SO and membrane potential. Anal Chem. 2023;95(15):6287–94.
51. Hu Q, Zhang S, Yang Y, Yao JQ, Tang WF, Lyon CJ. Extracellular vesicles in the pathogenesis and treatment of acute lung injury. Mil Med Res. 2022;9(1):61.
52. Tuckermann J, Adams RH. The endothelium–bone axis in development, homeostasis and bone and joint disease. Nat Rev Rheumatol. 2021;17(10):608–20.
53. Yin Hu, Zhang Y, Ni C-Y, Chen C-Y, Rao S-S, Yin H. Human umbilical cord mesenchymal stromal cells-derived extracellular vesicles exert potent bone protective effects by CLEC11A-mediated regulation of bone metabolism. Theranostics. 2020;10(5):2293–308.
54. Ambrosi TH, Marecic O, McArdle A, Sinha R, Gulati GS, Tong X. Aged skeletal stem cells generate an inflammatory degenerative niche. Nature. 2021;597(7875):256–62.
55. Torres HM, Arnold KM, Oviedo M, Westendorf JJ, Weaver SR. Inflammatory processes affecting bone health and repair. Curr Osteoporos Rep. 2023;21(6):842–53.
56. Court AC, Le-Gatt A, Luz-Crawford P, Parra E, Aliaga-Tobar V, Bátiz LF. Mitochondrial transfer from MSCs to T cells induces Treg differentiation and restricts inflammatory response. EMBO Rep. 2020;21(2):e48052.
57. Francesca V, Sarah E, Xavier D, Andres C, Yessia H, Maroun K. Mesenchymal stem cell-mediated transfer of mitochondria: mechanisms and functional impact. Cell Mole Life Sci. 2022;79(3):1–20.

58. Dejin Lu, Jiao X, Jiang W, Yang Li, Gong Q, Wang X. Mesenchymal stem cells influence monocyte/macrophage phenotype: regulatory mode and potential clinical applications. Biomed Pharmacother. 2023;165:115042.
59. Stephen E Alway, Hector G Paez, Christopher R Pitzer, Peter J Ferrandi, Mohammad Moshahid Khan, Junaith S Mohamed. Mitochondria transplant therapy improves regeneration and restoration of injured skeletal muscle. J Cachexia Sarcopenia Muscle. 2023;14(1):493–507.
60. Caryn M Cloer, Christopher S Givens, Lakisha K Buie, Lauren K Rochelle, Yi-Tzu Lin, Sam Popa. Mitochondrial transplant after ischemia reperfusion promotes cellular salvage and improves lung function during ex-vivo lung perfusion. J Heart Lung Transplant. 2023;42(5):575–584.
61. Zhang A, Liu Y, Pan J, Pontanari F, Chang AC, Wang H. Delivery of mitochondria confers cardioprotection through mitochondria replenishment and metabolic compliance. Mol Ther. 2023;31(5):1468–1479.
62. Malekpour K, Hazrati A, Soudi S, Hashemi SM. Mechanisms behind therapeutic potentials of mesenchymal stem cell mitochondria transfer/delivery. J Control Release. 2023;354:755–69.
63. Burt R, Dey A, Aref S, Aguiar M, Akarca A, Bailey K. Activated Stromal Cells Transfer Mitochondria to Rescue Acute Lymphoblastic Leukaemia Cells from Oxidative Stress. Blood. 2019;134(17):1415–29.
64. Nakao Y, Fukuda T, Zhang Q, Sanui T, Shinjo T, Kou X. Exosomes from TNF-α-treated human gingiva-derived MSCs enhance M2 macrophage polarization and inhibit periodontal bone loss. Acta Biomater. 2021;122:306–24.
65. Bastianello G, Porcella G, Beznoussenko GV, Kidiyoor G, Ascione F, Li Q. Cell stretching activates an ATM mechano-transduction pathway that remodels cytoskeleton and chromatin. Cell Rep. 2023;42(12): 113555.
66. Zhao H, Das BK, Wang L, Fujiwara T, Zhou J, Aykin-Burns N. Transferrin receptor 1-mediated iron uptake regulates bone mass in mice via osteoclast mitochondria and cytoskeleton. Elife. 2021;11: e73539.
67. Luz-Crawford P, Hernandez J, Djouad F, Luque-Campos N, Caicedo A, Carrère-Kremer S, Brondello J-M, Vignais M-L, Pène J, Jorgensen C. Mesenchymal stem cell repression of Th17 cells is triggered by mitochondrial transfer. Stem Cell Res Ther. 2019;10(1):232.
68. Gorospe CM, Carvalho G, Curbelo AH, Marchhart L, Mendes IC, Niedźwiecka K, Wanrooij PH. Mitochondrial membrane potential acts as a retrograde signal to regulate cell cycle progression. Life Sci Alliance. 2023;6(12): e202302091.
69. Liu F, Qiu H, Xue M, Zhang S, Zhang X, Xu J. MSC-secreted TGF-β regulates lipopolysaccharide-stimulated macrophage M2-like polarization via the Akt/FoxO1 pathway. Stem Cell Res Ther. 2019;10(1):1–14.
70. Kang Y, Song Y, Luo Y, Song J, Li C, Yang S. Exosomes derived from human umbilical cord mesenchymal stem cells ameliorate experimental non-alcoholic steatohepatitis via Nrf2/NQO-1 pathway. Free Radic Biol Med. 2022;192:25–36.

Publisher's Note